

# The Role of Regional SST Warming Variations in the Drying of Meso-America in Future Climate Projections\*

SARA A. RAUSCHER

*T-3 Fluid Dynamics, Los Alamos National Laboratory, Los Alamos, New Mexico*

FRED KUCHARSKI

*Earth System Physics Section, Abdus Salam International Centre for Theoretical Physics, Trieste, Italy*

DAVID B. ENFIELD

*Cooperative Institute for Marine and Atmospheric Studies, Rosenstiel School of Marine and Atmospheric Science, University of Miami, Miami, Florida*

(Manuscript received 23 November 2009, in final form 19 August 2010)

## ABSTRACT

This paper addresses several hypotheses designed to explain why AOGCM simulations of future climate in the third phase of the Coupled Model Intercomparison Project (CMIP3) feature an intensified reduction of precipitation over the Meso-America (MA) region. While the drying is consistent with an amplification of the subtropical high pressure cells and an equatorward contraction of convective regions due to the “upped ante” for convection in a warmer atmosphere, the physical mechanisms behind the intensity and robustness of the MA drying signal have not been fully explored. Regional variations in sea surface temperature (SST) warming may play a role. First, SSTs over the tropical North Atlantic (TNA) do not warm as much as the surrounding ocean. The troposphere senses a TNA that is cooler than the tropical Pacific, potentially exciting a Gill-type response, increasing the strength of the North Atlantic subtropical high. Second, the warm ENSO-like state simulated in the eastern tropical Pacific could decrease precipitation over MA, as warm ENSO events are associated with drying over MA.

The authors use the International Centre for Theoretical Physics (ICTP) AGCM to investigate the effects of these regional SST warming variations on the projected drying over MA. First, the change of SSTs [Special Report on Emissions Scenarios (SRES) A1B’s Twentieth-Century Climate in Coupled Model (A1B-20C)] in the ensemble average of the CMIP3 models is applied to determine if the ICTP AGCM can replicate the future drying. Then the effects of 1) removing the reduced warming over the TNA, 2) removing the warm ENSO-event-like pattern in the eastern tropical Pacific, and 3) applying uniform SST warming throughout the tropics are tested. The ICTP AGCM can reproduce the general pattern and amount of precipitation over MA. Simulations in which the CMIP3 A1B-20C ensemble-average SSTs are added to climatological SSTs show drying of more than 20% over the MA region, similar to the CMIP3 ensemble average. Replacing the relatively cooler SSTs over the TNA excites a Gill response consistent with an off-equatorial heating anomaly, showing that the TNA relative cooling is responsible for about 16% (31%) of the drying in late spring (early summer). The warm ENSO-like SST pattern over the eastern Pacific also affects precipitation over the MA region, with changes of 19% and 31% in March–June (MMJ) and June–August (JJA), respectively. This work highlights the importance of understanding even robust signals in the CMIP3 future scenario simulations, and should aid in the design and analysis of future climate change studies over the region.

---

\* Los Alamos National Laboratory Publication Number LA-UR 09-07079.

---

*Corresponding author address:* Sara Rauscher, T-3 Fluid Dynamics, Los Alamos National Laboratory, MS B216, Los Alamos, NM 87545.  
E-mail: rauscher@lanl.gov

## 1. Introduction

One of the most robust climate change signals in the models of the third phase of the Coupled Model Intercomparison Project (CMIP3) (Meehl et al. 2007b) used for the Fourth Assessment Report (AR4) of the Intergovernmental Panel on Climate Change (IPCC) is

a projected future drying over the Meso-America (MA) region including Central America, southern Mexico, and the Caribbean (Giorgi 2006; Neelin et al. 2006; Rauscher et al. 2008; Maurer et al. 2009). In the future scenario simulations, precipitation decreases by as much as 25%, with the largest decreases in June and July, the beginning of the core rainy season for much of MA. Large-scale circulation features associated with this late spring and early summer [May–July (MJJ)] drying include a southward displacement of the eastern Pacific ITCZ, stronger low-level easterlies (Vecchi and Soden 2007), and a more intense Caribbean low-level jet (CLLJ) (Rauscher et al. 2008). In association with these strong easterlies, the North Atlantic subtropical high (NASH) expands westward early and intensifies compared with twentieth-century climatology. The stronger NASH is associated with lower relative humidity, anomalous subsidence, and increased low-level divergence that discourage convection in the early part of the rainy season (Vecchi and Soden 2007; Cook et al. 2008; Rauscher et al. 2008).

The decrease in precipitation and changes in the NASH are consistent with a general intensification and poleward movement of the subtropical high pressure cells noted in observations and models (Christensen et al. 2007), and perhaps with an equatorward contraction of tropical convective regions due to the “upped ante” for convection in a warmer, more stable atmosphere (Neelin et al. 2003; Chou and Neelin 2004). However, the drying over MA is particularly robust compared to other regions on convective margins (Neelin et al. 2006). The question of why MA is the strongest climate change “hot spot” (Giorgi 2006) (or in this case, “dry spot”) in the tropics and subtropics requires further exploration.

The pattern of SST warming in the tropics and subtropics has recently emerged as an important factor in the regional response to greenhouse-gas-induced climate change (Xie et al. 2010; Clement et al. 2010). Since the tropical-mean SST will determine upper-tropospheric temperature changes, areas where SSTs do not warm as much will have greater static stability and vice versa (Sobel et al. 2002; Chiang and Sobel 2002). This may be the case over the tropical North Atlantic (TNA) where there is less warming compared to the global tropical strip (Vecchi and Soden 2007; Leloup and Clement 2009). This reduced warming over the TNA is a robust feature in AOGCMs that is the result of “the influence of the climatological wind speed on the efficiency of the latent heat flux: it is easy to cool off windy regions resulting in a smaller SST change” (Leloup and Clement 2009; Xie et al. 2010). The reduced warming over the TNA vis-à-vis other tropical ocean basins could excite a Gill-type response (Gill 1980), enhancing surface divergence and increasing the strength of the NASH and potentially the

strength of the Caribbean low-level jet (Wang and Lee 2007; Wang et al. 2007, 2008). In fact, several of the CMIP3 models show a Gill-type response to the warming minimum, with low-level anticyclonic circulations and upper-level cyclonic circulation to the northwest of the area of reduced warming (Rauscher et al. 2008). In contrast to the TNA, the tropical eastern Pacific warms more than the zonal mean. Such a warm ENSO-event-like state in the eastern tropical Pacific could reduce precipitation over MA, as warm ENSO events are associated (although weakly) with drying over the MA region and a more southerly position of the eastern Pacific ITCZ (Hastenrath 1976, 1978; Ropelewski and Halpert 1987; Enfield 1996; Waylen et al. 1996; Enfield and Mayer 1997; Giannini et al. 2000; Curtis 2002; Hastenrath 2002; Magaña et al. 2003).

Here we make use of the International Centre for Theoretical Physics (ICTP) AGCM (Molteni 2003) to investigate the effects of the differential warming in the tropical North Atlantic and the eastern tropical Pacific on the projected drying over MA. First, we apply the change in SSTs [Special Report on Emissions Scenarios (SRES) A1B Twentieth-Century Climate in Coupled Models (20C3M), hereafter A1B-20C] from the ensemble average of 17 of the CMIP3 models to determine if the ICTP AGCM can replicate the future drying signal found in many of the CMIP3 models. Then we test the effects of 1) removing the reduced warming over the tropical North Atlantic, 2) removing the warm ENSO-event-like pattern in the eastern tropical Pacific, and 3) applying uniform SST warming over the tropics and subtropics. In these experiments, CO<sub>2</sub> concentrations are kept constant so that the climate response to the applied SST forcing may be isolated. Of course, in the CMIP3 runs the ensemble-mean SST increase in the twenty-first century is a consequence of the greenhouse gas (GHG) forcing from the A1B scenario. Nonetheless, Stephenson and Held (1993) argue that CO<sub>2</sub> affects the atmosphere, both directly through changes in radiative heating and cooling rates (directly) and also indirectly by changing SSTs. The main additional direct effects of the CO<sub>2</sub> absorption change on the model climate are a stratospheric cooling, a moderate increase in land surface temperatures, and a positive Arctic Oscillation response (e.g., Bracco et al. 2004). However, the indirect effect appears to overcome the direct effect. An additional simulation in which CO<sub>2</sub> absorption in the longwave spectrum is increased is performed for comparison.

In section 2 we detail the models, data, and experimental setup. Section 3 describes the results of the experiments, focusing on precipitation, sea level pressure (SLP), and the 925-hPa and 200-hPa circulation. Finally, section 4 presents the discussion and conclusions.

## 2. Methods

### a. ICTP AGCM

The model used in this study is the ICTP AGCM (Molteni 2003). It is based on a hydrostatic spectral dynamical core (Held and Suarez 1994) and uses the vorticity divergence form described by Bourke (1974). The parameterized processes include shortwave and longwave radiation; large-scale condensation; convection; surface fluxes of momentum, heat, and moisture; and vertical diffusion. Convection is represented by a mass flux scheme that is activated where conditional instability is present, and boundary layer fluxes are obtained by stability-dependent bulk formulae. A simple one-layer thermodynamic model determines land and ice temperatures. In this study, the ICTP AGCM is configured with eight vertical ( $\sigma$ ) levels [an improvement to the model version presented by Molteni (2003), which used five] and with a spectral truncation at total wavenumber 30. Applications of the ICTP AGCM can be found in Bracco et al. (2005) and Kucharski et al. (2006a,b, 2009).

### b. Data

The SST forcing data come from two sets of CMIP3 simulations (Meehl et al. 2007b); as a control, we use the 20C3M (referred to here as 20C). The 20C experiments originate from preindustrial control runs. In those runs, historical measurements of greenhouse gases, sulfate aerosols, and solar and volcanic forcings are applied for the twentieth century. For the future climate projection, we analyze the emission scenario A1B (Nakicenovic and Swart 2000), which uses medium-high carbon emissions (between 1450 and 1800 GtC) and carbon dioxide concentrations (700 ppm by 2100) to be consistent with the analysis of Rauscher et al. (2008). Although we focus on one scenario, previous work has indicated that regional precipitation change patterns are relatively insensitive to the scenario (Giorgi and Bi 2005). We compare two periods: 1961–90 (twentieth century) and 2061–90 (twenty-first century). We add the delta of the ensemble average SSTs (A1B-20C) from 17 models [see Table 1 in Rauscher et al. (2008)] to climatological observed SSTs derived from the European Centre for Medium-Range Weather Forecasts reanalysis (see Molteni 2003).

Model performance in simulating precipitation is evaluated using observed data from two gridded monthly precipitation datasets: the Climate Prediction Center Merged Analysis of Precipitation (CMAP) (Xie and Arkin 1996) and the Global Precipitation Climatology Project (GPCP) dataset (Huffman et al. 2009). Both are blended products of global satellite and gauge data on a  $2.5^\circ$  latitude–longitude grid. We employ these fairly coarse-resolution

data because they have coverage over both land and ocean and also because their grid spacing is similar to that employed by the ICTP AGCM, which at T30 is approximately  $3.8^\circ$  latitude  $\times$  longitude. We use the period 1979–2002. Simulated SLP and wind data are compared with the National Centers for Environmental Prediction–National Center for Atmospheric Research (NCEP–NCAR) reanalysis project (NNRP) (Kalnay et al. 1996).

### c. Experiments

A set of six experiments, each 100 years in length, is performed with the ICTP AGCM. The control experiment (CTL) is run with an observed climatology of SSTs with no interannual variability except an annual cycle. In experiment A1B we add the delta SST (A1B-20C) to the climatological observed SSTs described in the previous section. The applied deltas are a 30-yr climatology, but the annual cycle is retained. The applied SST warming (annual average) for experiment A1B is shown in Fig. 1a. For completeness, we perform an experiment in which the longwave absorption of  $\text{CO}_2$  exponentially increases with 1950 as a reference, resulting in about a 50% increase in 100 yr (A1BCO2, not shown since the SST configuration is the same as in experiment A1B).

To determine the effects of the reduced warming over the TNA [see Fig. 4c in Vecchi and Soden (2007)], we add the difference between the zonal mean and each grid point for a box covering the area  $10^\circ$ – $30^\circ\text{N}$ ,  $100^\circ$ – $15^\circ\text{W}$  [anomaly with one times the zonal mean difference (ANOM1Z), Fig. 1b]. Grid points to the west of the Central American isthmus in the Pacific Ocean were excluded. In this way the SSTs are made equivalent to the zonal-mean warming over the region. The month in which the SST warming is the lowest compared to the zonal average is shown in Fig. 2a. Maximum differences occur in late spring and early summer in many regions, although the Gulf of Mexico shows greater differences in winter (Fig. 2b). To exaggerate the effects of this experiment and to explore the consequences of an opposite zonal contrast between the Atlantic and Pacific Oceans, we add four times the zonal mean difference, creating a warm SST anomaly (SSTA) over the same region (ANOM4Z, Fig. 1c). Hence, we use ANOM1Z to assess the importance of the relative cooling in the Atlantic (i.e., a quantitative assessment), whereas the larger amplitude experiment, ANOM4Z, pinpoints the physical mechanism in more detail. Note that the largest SST changes imposed in ANOM1Z and ANOM4Z are located in the eastern part of the Atlantic warm pool (AWP), the Gulf of Mexico, Caribbean Sea, and western tropical Atlantic. Therefore, our SST changes are slightly different in location and magnitude than those employed in studies that directly examine the effect of the AWP on climate

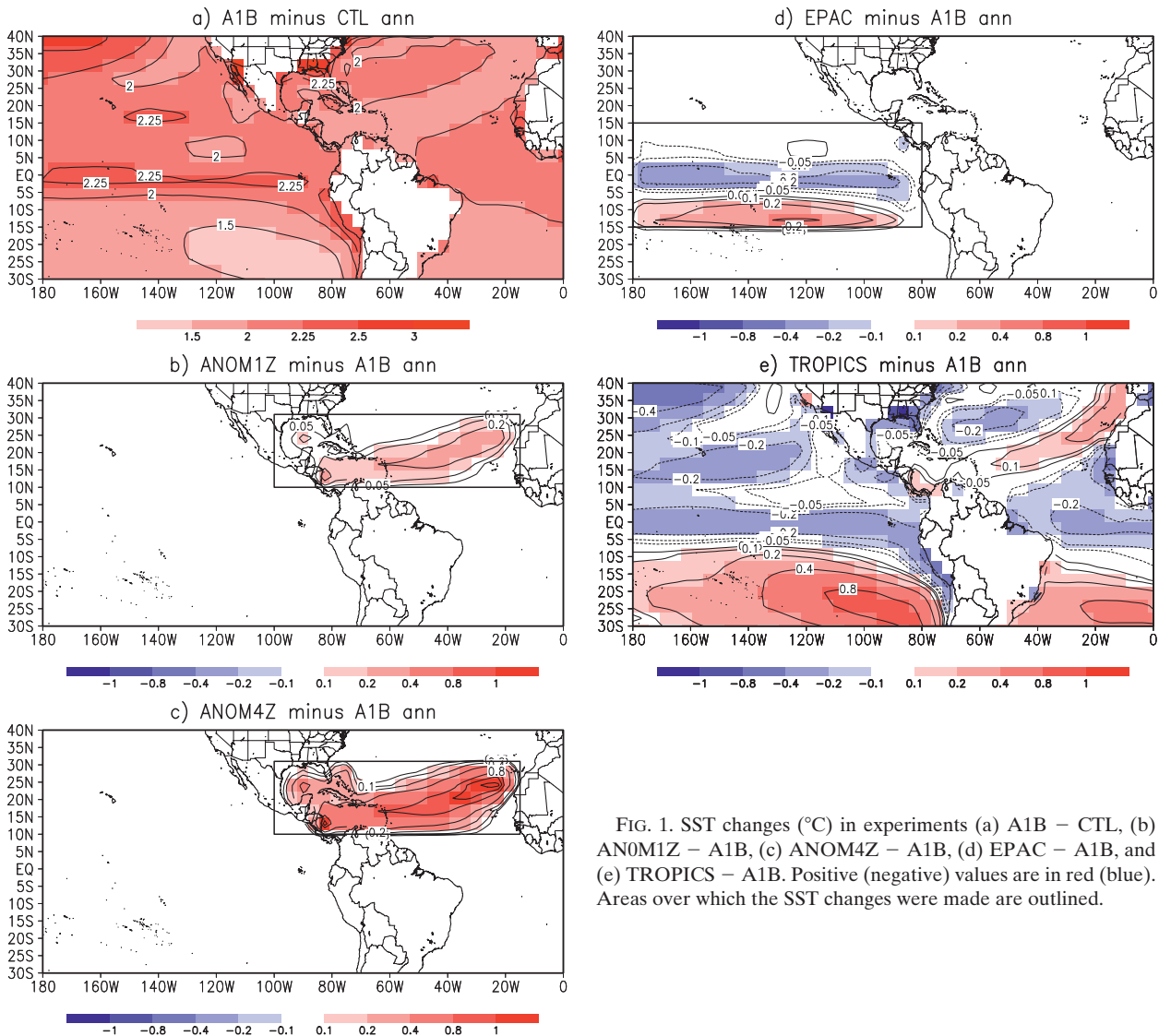


FIG. 1. SST changes ( $^{\circ}\text{C}$ ) in experiments (a) A1B – CTL, (b) ANOM1Z – A1B, (c) ANOM4Z – A1B, (d) EPAC – A1B, and (e) TROPICS – A1B. Positive (negative) values are in red (blue). Areas over which the SST changes were made are outlined.

(Wang et al. 2007, 2008). In those AWP experiments, the imposed SST changes are confined west of  $40^{\circ}\text{W}$  [see Fig. 1 in Wang et al. (2007, 2008)], with maximum differences located around the island of Cuba. In contrast, in our experiments the largest differences are located farther east, around  $20^{\circ}\text{W}$ .

Two additional experiments are performed to identify the effects of uniform warming over the tropical strip and to isolate the effects of the warm ENSO-like pattern in the eastern tropical Pacific. In experiment TROPICS, a uniform warming of approximately 2 K (the average warming over the region  $40^{\circ}\text{S}$ – $40^{\circ}\text{N}$ ,  $0^{\circ}$ – $360^{\circ}$ ) is applied to the spatially varying climatology. This allows us to assess the upped ante effect and its contribution to the drying over the MA region. To investigate the effects of the warm ENSO-like SST pattern in the eastern Pacific

(experiment EPAC), we compute the area-average difference (A1B–20C) over  $15^{\circ}\text{S}$ – $15^{\circ}\text{N}$ ,  $180^{\circ}$ – $80^{\circ}\text{W}$ , and then add this difference to the climatological SSTs over the same region ( $15^{\circ}\text{S}$ – $15^{\circ}\text{N}$ ,  $180^{\circ}$ – $80^{\circ}\text{W}$ ). This removes the warm anomaly along the equator and the cool anomaly near  $10^{\circ}\text{S}$ ,  $120^{\circ}\text{W}$  (Fig. 1d).

### 3. Results

#### a. Model climatology

First, we examine the annual cycle of precipitation to determine whether the ICTP model can reproduce the precipitation climatology for the region. For the annual cycle analysis, we define the Meso-America region as  $9^{\circ}$ – $24^{\circ}\text{N}$ ,  $95^{\circ}$ – $60^{\circ}\text{W}$ , which includes Central America, southern Mexico and the Yucatan Peninsula, and the

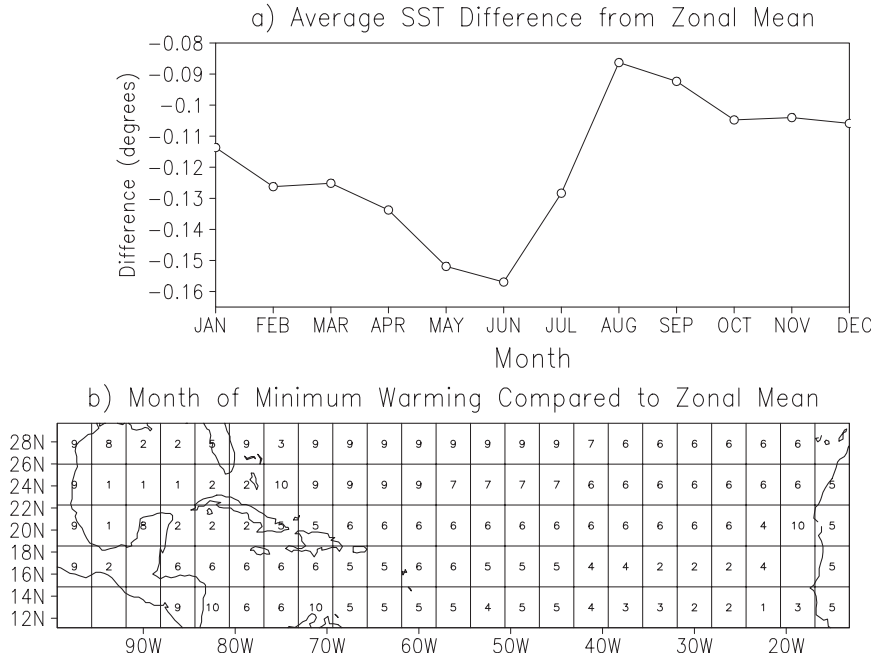


FIG. 2. Monthly average SST differences ( $^{\circ}\text{C}$ ) from (a) zonal mean over ANOM1Z area and (b) month of maximum deviation from zonal-mean precipitation difference (A1B – 20C).

western Caribbean. Over much of this region, the rainy season extends from May to October with maxima in June and September/October and slightly lower precipitation totals in July and August (Hastenrath 1967). This period of lower rainfall is called the midsummer drought (MSD) (Magaña et al. 1999).

Figure 3 shows that the ICTP CTL simulates the precipitation annual cycle fairly well, although precipitation is overestimated compared to observations and is shifted late by about one month. The 20C CMIP3 ensemble average is shown for comparison. Almost all of the CMIP models underestimate precipitation over this region (Dai 2006; Rauscher et al. 2008), due in part to a SST cold bias of  $1^{\circ}$ – $2^{\circ}\text{C}$  in the Intra-Americas Sea (IAS) region (Dai 2006). One noticeable feature is the wet bias of the ICTP AGCM versus the dry bias of the CMIP3 models. This difference is consistent with previous comparisons of CMIP versus the Atmospheric Model Intercomparison Project (AMIP) simulations of tropical precipitation (e.g., Covey et al. 2003; Lin 2007).

Now we assess the ICTP AGCM precipitation climatology for MJJ since this is the time of the year that shows the most pronounced future drying. Figure 4a shows GPCP precipitation climatology, while the ICTP AGCM is shown in Fig. 4b. The climatology of the GPCP data is very similar to the CMAP data, so the latter are not shown here. The ICTP AGCM has a spatial pattern of precipitation that resembles the observations. The

eastern Pacific ICTZ precipitation tends to be too intense in the model, although the latitudinal position is similar to observations (if a little too narrow). The Atlantic ITCZ is located too far south and appears to be somewhat discontinuous, a feature seen in other AGCMs such as ECHAM (Rauscher et al. 2007). However, both

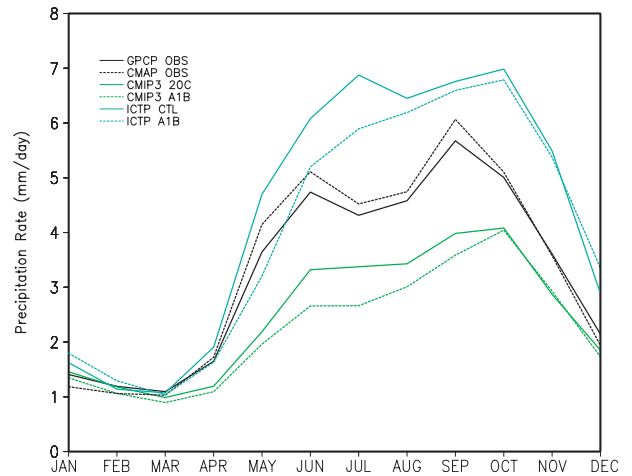


FIG. 3. Annual cycle of average precipitation ( $\text{mm day}^{-1}$ ) for CMAP (solid black) and GPCP (short dashed black) observations, ensemble average of CMIP3 20C simulations (green), the ensemble average of the CMIP3 A1B simulations (green dashed), CTL simulation for the ICTP AGCM (blue), and A1B simulation for the ICTP AGCM simulation (blue dashed) for MA ( $9^{\circ}$ – $24^{\circ}\text{N}$ ,  $95^{\circ}$ – $60^{\circ}\text{W}$ ).

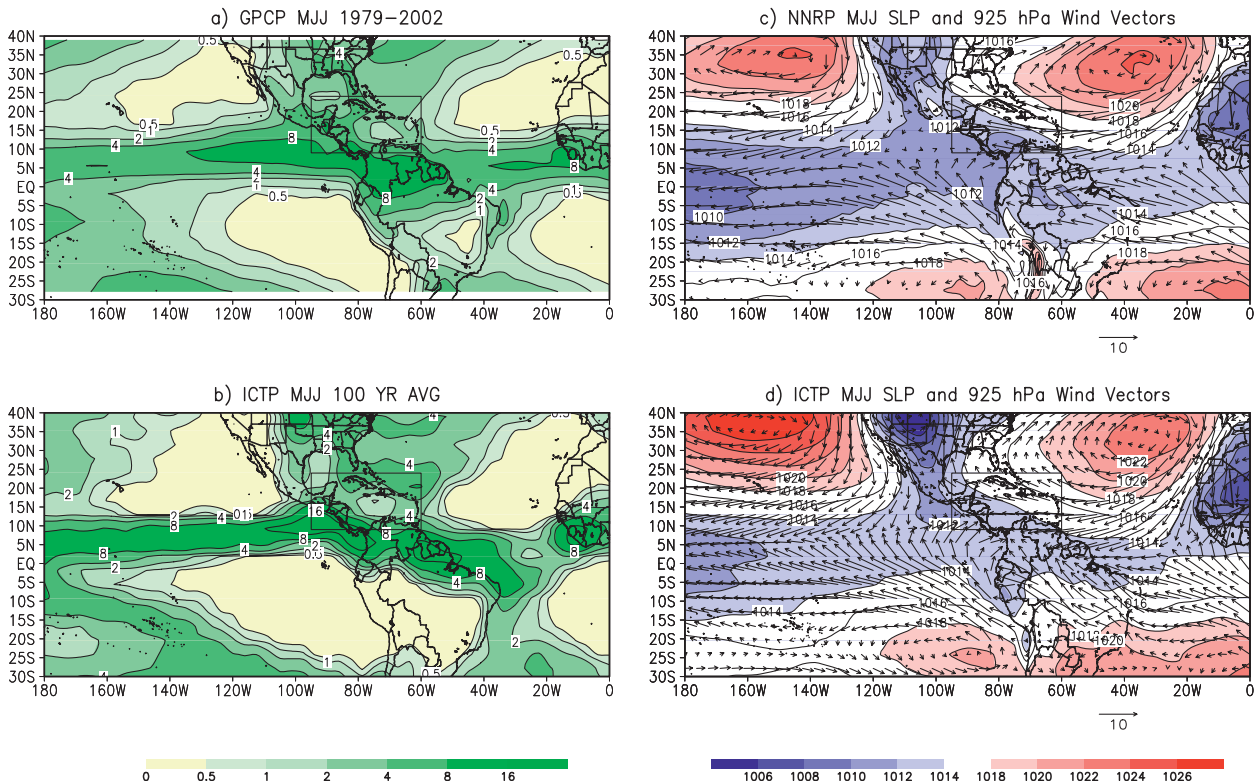


FIG. 4. Average MJJ seasonal precipitation rate ( $\text{mm day}^{-1}$ ) for (a) GPCP data (1979–2002) and (b) ICTP AGCM, and seasonal SLP (hPa) and 925-hPa winds ( $\text{m s}^{-1}$ ) for (c) NNRP data (1968–96) and (d) ICTP AGCM.

the ICTP AGCM simulation and the GPCP observations show slight precipitation minima over the Gulf of Mexico and the Caribbean Sea. Examining the ICTP AGCM depiction of the low-level circulation (Fig. 4d), we see that the NASH does not extend far enough westward toward the North American continent. The circulation around the NASH is well simulated, with a suggestion of the Caribbean low-level jet, a maximum in easterly winds located near 15°N, 70°–80°W (Amador 1998; Wang and Lee 2007; Wang 2007). Over the tropical eastern Pacific, SLP is generally too high east of 160°W from 10°S to 10°N, but the winds converge at about 5°N in both the NNRP (Fig. 4c) and the ICTP AGCM, although the convergence appears to be stronger in the ICTP AGCM, which may be related to the narrow ITCZ.

### b. Experiment A1B

Comparing the annual cycle of precipitation between the ICTP-modeled A1B and CTL simulations (Fig. 3), precipitation decreases throughout most of the year in the ICTP AGCM A1B experiment. The precipitation changes are concentrated over the early part of the rainy season and the MSD, with a maximum change in May for the ICTP AGCM and in July for the CMIP3 ensemble average. This is also the period when the SST

warming minimum is most pronounced in the tropical Atlantic (Fig. 2). Figure 5a shows the spatial map for the difference in precipitation for MJJ for A1B – CTL. For all results, unless otherwise indicated, shaded regions are significant at the 90% level using a Student's *t* test. Similar to the CMIP3 model results (see Fig. 9 in Rauscher et al. 2008), drying is present over MA, with decreases in precipitation of more than 20% over Central America and larger decreases over the tropical Atlantic in the region that corresponds to the SST warming minimum (10°–25°N, 60°–20°W). It is interesting that the ICTP AGCM captures the drying over the MA region with SST forcing alone and without increasing greenhouse gas concentrations, although the drying is accentuated over the Caribbean if the longwave absorption effects of CO<sub>2</sub> increases are included, as in experiment A1BCO2 (Figs. 6a,b). If the SST forcing alone is enough to drive the precipitation changes, this implies that the main effect (or most relevant for the processes under investigation) of GHG forcing is to initially change SSTs and then influence the rainfall.

However, the SLP response (Fig. 7a) in the ICTP AGCM is somewhat out of sync with the CMIP3 model results. While SLP does increase in the MA region, consistent with the CMIP3 models, SLP also increases

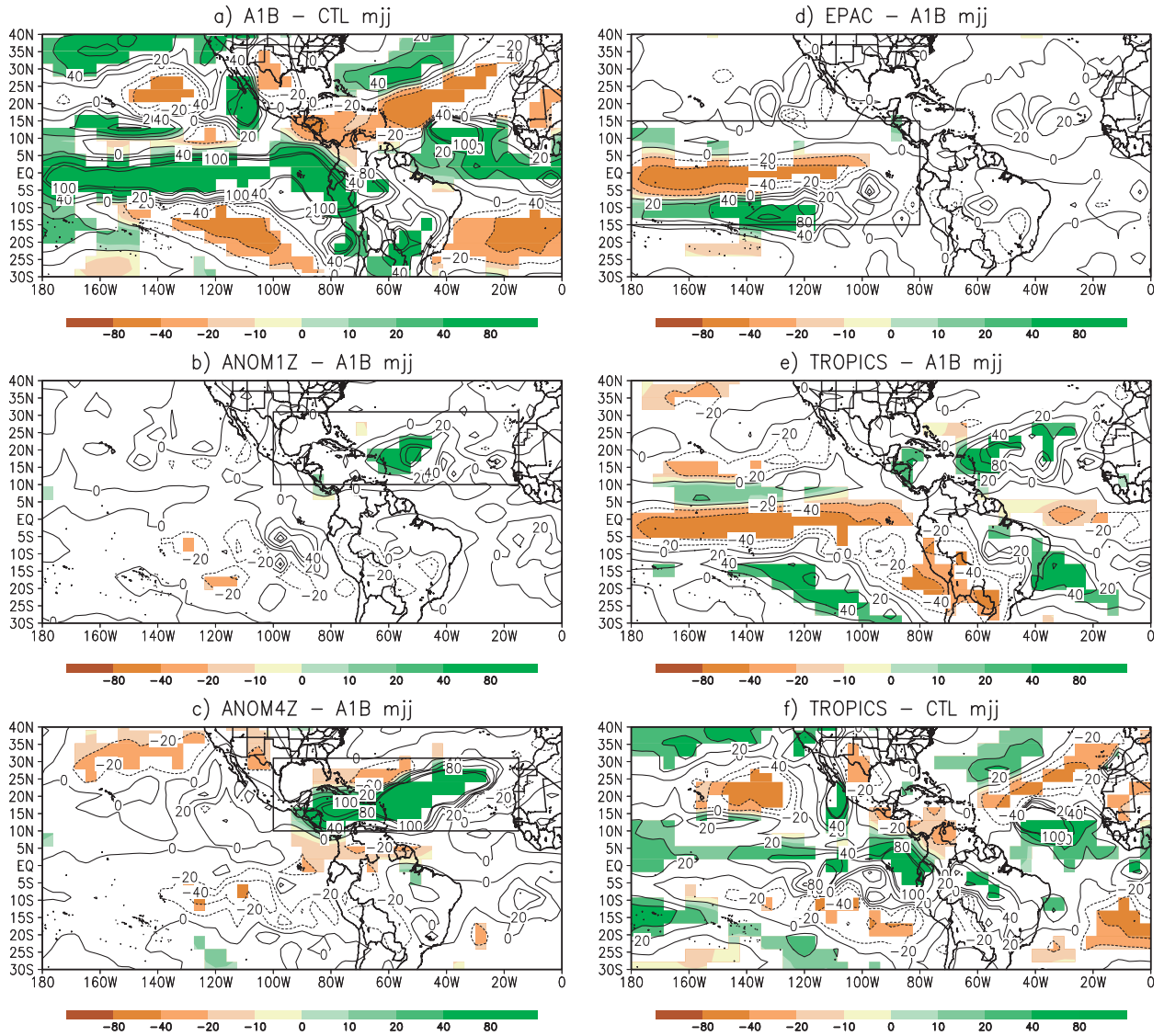


FIG. 5. Average MJJ percent differences in precipitation for (a) A1B - CTL, (b) ANOM1Z - A1B, (c) ANOM4Z - A1B, (d) EPAC - A1B, (e) TROPICS - A1B, and (f) TROPICS - CTL. Positive (negative) values are in green (brown). Shaded areas are significant with  $\alpha = 0.10$ . Contour interval is from -100% to 100% at 20% increments.

over all of North America. In addition, there is an apparent decrease in the strength of the NASH, opposite of what is seen in the CMIP3 ensemble average, and the NASH does not move westward early in the A1B experiment compared to the CTL (not shown). These differences are likely due to the absence of GHG increase in the experimental setup, which decreases the warming over the North American continent and reduces the land-sea contrast between North America and the Gulf of Mexico/tropical Atlantic. In an additional experiment that includes the effects of higher longwave absorption of  $\text{CO}_2$  (A1BCO2), SLP increases in the area of the NASH (Fig. 6d) when compared to the A1B experiment.

### c. Experiments ANOM1Z and ANOM4Z

In MJJ, both ANOM1Z and ANOM4Z show precipitation increases over the SST forcing region (Figs. 5b,c). Despite the small forcing applied in ANOM1Z ( $0.1^\circ\text{--}0.2^\circ$ ), there are statistically significant increases in precipitation of up to 80% compared to the A1B experiment over a small area near  $20^\circ\text{N}$ ,  $60^\circ\text{W}$ . To quantify the relative contribution of the reduced warming over TNA to the drying over the Meso-America region defined in section 3a, we compare the area-averaged seasonal precipitation differences for ANOM1Z and A1B versus the CTL experiment, that is,  $1 - [(\text{ANOM1Z} - \text{CTL})/(\text{A1B} - \text{CTL})]$ ,

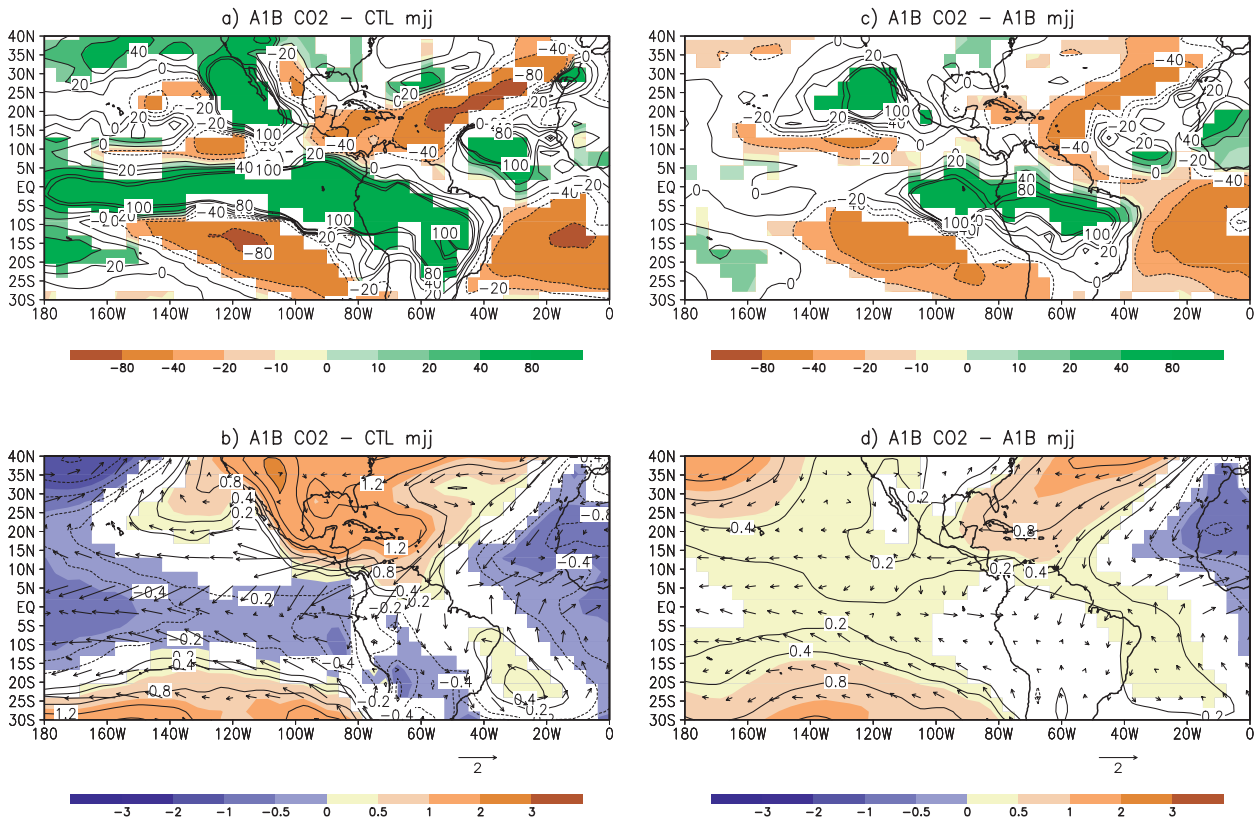


FIG. 6. Average MJJ differences in precipitation (percent) (a),(c) SLP and (b),(d) 925-hPa winds ( $\text{m s}^{-1}$ ) (a),(b) A1BCO<sub>2</sub> - CTL and (c),(d) A1BCO<sub>2</sub> - A1B. Shaded areas are significant with  $\alpha = 0.10$ .

and find that in MJJ the TNA warming minimum accounts for about 16% of the drying. In June–August (JJA) this amount increases to 31%. The magnitude and spatial extent of the increase in precipitation are greater in ANOM4Z, with precipitation changes of up to and more than 100% (ANOM4Z - A1B) in some grid boxes. In fact, when ANOM4Z - CTL (Fig. 8) is compared to A1B - CTL (Fig. 5a), much of the drying over the Caribbean Sea disappears or is even reversed. The ANOM4Z experiment also displays increased drying to the north and south of the wetter region compared to the A1B simulation, as exemplified by an amplified drying signal over northern Mexico and Texas. The precipitation effects of the applied SST anomalies in ANOM1Z and ANOM4Z do not appear to extend far out into the Pacific. The response in JJA is similar, although ANOM1Z shows positive precipitation response west of Central America that is not present in MJJ, suggesting slightly more remote (or far reaching) effects of the applied forcing (not shown).

Considering the circulation response in ANOM4Z and ANOM1Z compared to A1B, in MJJ SLP decreases over the region of applied forcing (Figs. 7b,c); the effect is greater in ANOM4Z than in ANOM1Z, so we turn

our attention to ANOM4Z to better identify the physical mechanism at work. Associated with the SLP decrease is a low-level cyclonic circulation shown as a negative anomaly in the 925-hPa streamfunction and wind vectors (Fig. 9a). These results are qualitatively similar to those of Enfield et al. (2006) and Wang et al. (2007, 2008), who tested the effects of the Atlantic warm pool on the circulation in the Caribbean and found that a warmer/larger Atlantic warm pool tends to reduce the strength of the NASH. At the 200-hPa level (Fig. 9b), there is a positive eddy streamfunction anomaly and an anticyclonic circulation to the north and west of the heating anomaly. The presence of this baroclinic structure close to the imposed SST forcing is consistent with a Gill response to an off-equatorial heating anomaly (Gill 1980). Following the steady, linearized vorticity equation (Gill 1980), a negative heating anomaly and associated column shrinking would be balanced by equatorward motion to the west of the forcing. Therefore, a Gill response to a cold anomaly is characterized by a low-level anticyclone to the west of the cooling and an upper-level cyclone, thus providing a baroclinic structure. This part may be interpreted as the Rossby wave part of the response. An examination of the 200-hPa velocity potential ( $\chi$ ) and divergent wind

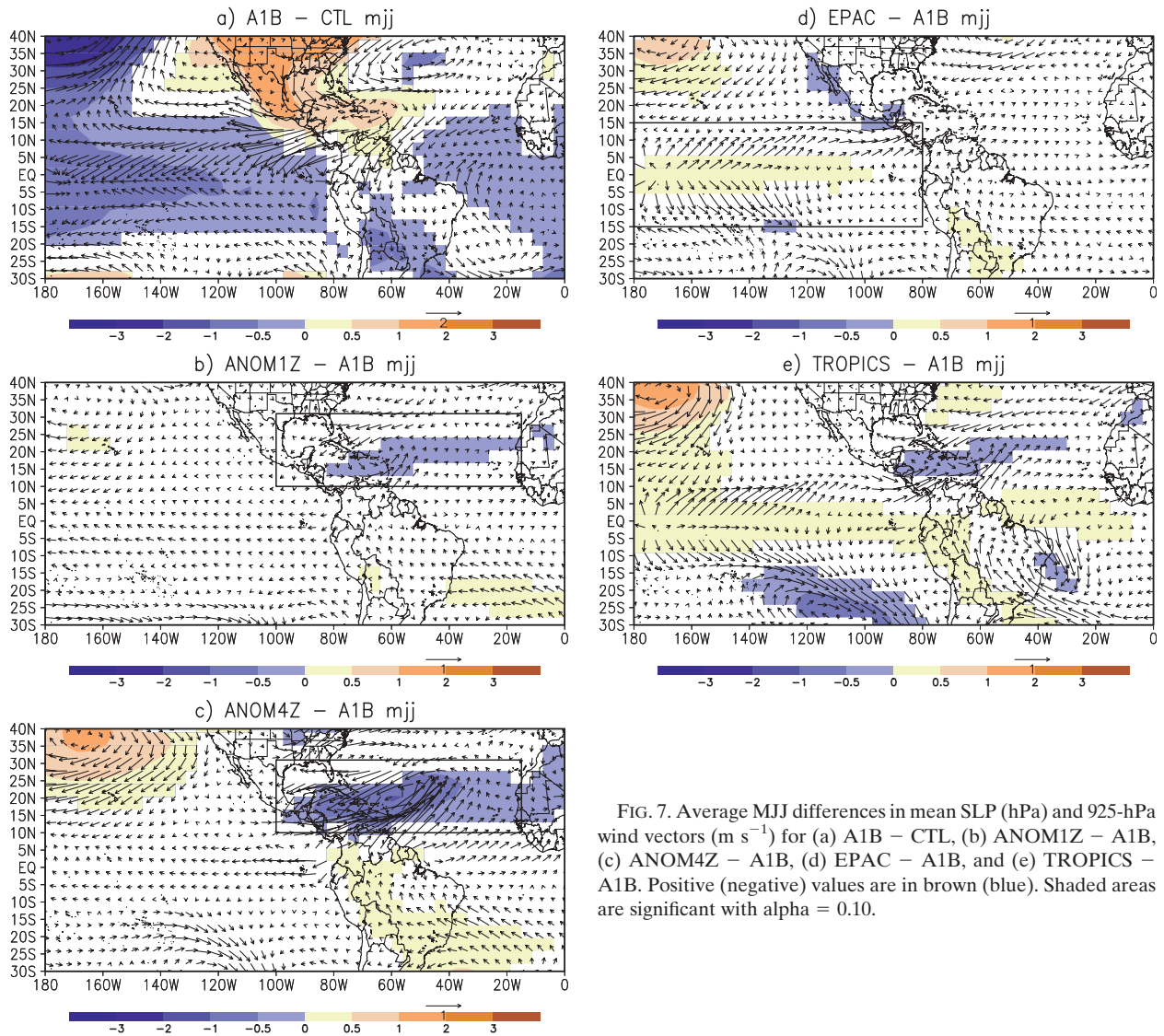


FIG. 7. Average MJJ differences in mean SLP (hPa) and 925-hPa wind vectors ( $\text{m s}^{-1}$ ) for (a) A1B – CTL, (b) ANOM1Z – A1B, (c) ANOM4Z – A1B, (d) EPAC – A1B, and (e) TROPICS – A1B. Positive (negative) values are in brown (blue). Shaded areas are significant with  $\alpha = 0.10$ .

anomalies (Fig. 9c) indicate a negative  $\chi$  anomaly in the vicinity of the strongest forcing with associated upper-level divergence and a positive  $\chi$  anomaly to the west. In JJA, the pattern is shifted slightly with the negative  $\chi$  anomalies extending farther west (not shown). Farther away from the forcing, and in particular in the northern extratropics, the response is complex and may be related to circuglobal teleconnections associated with the jet stream waveguide (Branstator 2002). A detailed analysis of this response is beyond the scope of this paper.

Although we cannot examine directly the effect of the SST pattern on tropical cyclones (TCs), we can look at related dynamical factors. Figure 10 shows the difference in vertical wind shear, calculated as the absolute value of the difference between the 850- and 200-hPa zonal wind. The full difference field is shown here. Both

ANOM1Z and ANOM4Z (Figs. 10b,c) show a decrease in vertical wind shear relative to the A1B experiment. Several studies have indicated that higher vertical wind shear in the future scenario CMIP3 simulations may actually act to inhibit or reduce TC formation over the TNA despite the higher SSTs over the region (Vecchi and Soden 2007; Knutson et al. 2008). Our result suggests that this increase in vertical wind shear may be partly dependent on the SST pattern. However, while TCs are important extreme events, their contribution to the quantities analyzed here, monthly and seasonal average precipitation, may not be large. Considering areas similar to our Meso-America region, the TC contribution to area-averaged precipitation over the MA region is less than 3% during the early part of hurricane seasons (June–July) (e.g., Rodgers et al. 2001; Jiang and Zipser 2010).

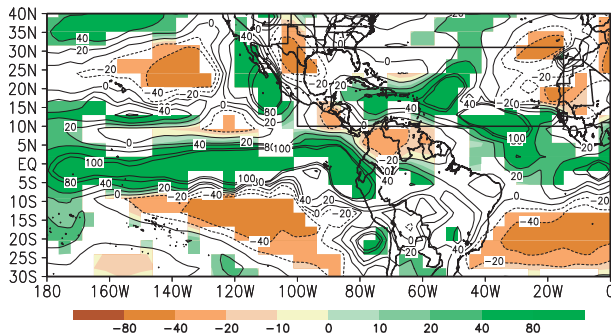


FIG. 8. Average MJJ percent differences in precipitation for ANOM4Z – CTL for MJJ. Positive (negative) values are in green (brown). Shaded areas are significant with  $\alpha = 0.10$ . Contour interval is from  $-100\%$  to  $100\%$  at  $20\%$  increments.

In summary, the ANOM1Z and ANOM4Z experiments illustrate how the reduced warming in the TNA affects the CMIP3 simulations. Because the TNA warms less than the Pacific, the troposphere senses a TNA that is cooler than the Pacific and interprets this as a small warm pool situation within the global context, responding as if to a small warm pool situation with high SLP, a strong CLLJ, less MA rainfall, and stronger vertical wind shear over the main TC development region over the IAS (Enfield et al. 2006; Wang et al. 2007, 2008).

#### d. Experiments EPAC and TROPICS

Because of the presence of a warm ENSO-like pattern in the eastern tropical Pacific, we also test the effects of removing this meridional SST pattern (cool anomaly at  $10^{\circ}$ – $15^{\circ}$ S and a warm anomaly near the equator) by replacing SSTs in this region with the area-average warming. This experiment significantly increases precipitation over the Central American isthmus in MJJ (Fig. 5d) and JJA (not shown). Overall, this change contributes 19% of the drying in MJJ and 31% in JJA, that is,  $1 - (\text{EPAC} - \text{CTL})/(\text{A1B} - \text{CTL})$ , similar to ANOM1Z.

The circulation changes associated with these precipitation changes are consistent with patterns that favor wetter conditions over MA, particularly over the Central American isthmus. Figure 7d shows a SLP decrease throughout the MA region. Moreover, the low-level divergence in the vicinity of the applied cooler SSTs near the equatorial eastern Pacific results in anomalous southwesterly cross-equatorial flow toward the western side of the Central American isthmus that is normally associated with wet conditions, especially on the Pacific side of the Sierra Madre (Hastenrath 1967; Waylen et al. 1996; Peña and Douglas 2002). If more realistic topography were used, there could be an even greater precipitation response, as the southwesterly cross-equatorial flow would rise up over the rugged terrain, generating

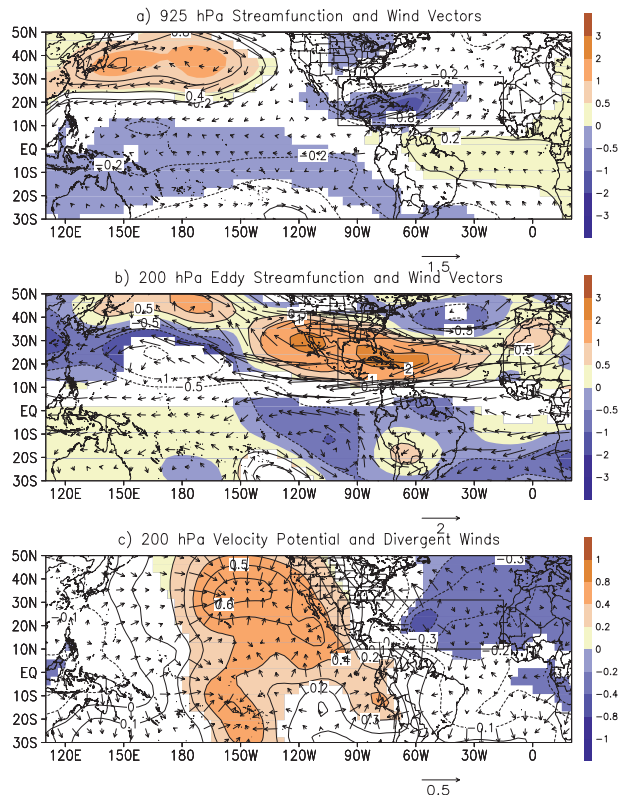


FIG. 9. Average MJJ differences for ANOM4Z-A1B for (a) 925-hPa streamfunction ( $10^6 \text{ m}^2 \text{ s}^{-1}$ ) and wind vectors ( $\text{m s}^{-1}$ ), (b) 200-hPa eddy streamfunction ( $10^6 \text{ m}^2 \text{ s}^{-1}$ ) and wind vectors ( $\text{m s}^{-1}$ ), and (c) 200-hPa velocity potential ( $10^6 \text{ m}^2 \text{ s}^{-1}$ ) and divergent winds ( $\text{m s}^{-1}$ ). Shaded areas are significant at  $\alpha = 0.1$ .

precipitation. Our experiments are consistent with observations, where it has been shown that during warm (cold) ENSO events, less (more) rainfall occurs on the Pacific coast of Central America because the easterly CLLJ across the isthmus is strengthened (weakened) when the SSTA gradient from the Pacific to the Atlantic is negative (positive), resulting in a stronger (weaker) pressure gradient across the isthmus (Enfield and Alfaro 1999). At 200 hPa, the EPAC experiment (Fig. 11a) shows that removing the warm ENSO-like pattern appears to strengthen the east–west Walker circulation, with negative anomalies in  $\chi$  over the western tropical Pacific and enhanced upper-level convergence over the central and eastern Pacific. Moreover, as in the ANOM1Z and ANOM4Z, there is a decrease in vertical wind shear (Fig. 10d) when the warm ENSO-like pattern is removed. This result is in agreement with the increase in vertical wind shear that occurs during warm ENSO events (Gray 1984).

The results of the TROPICS experiment are qualitatively similar to combining the EPAC and ANOM1Z experiments, with changes in precipitation over the eastern tropical Pacific and an increase in precipitation

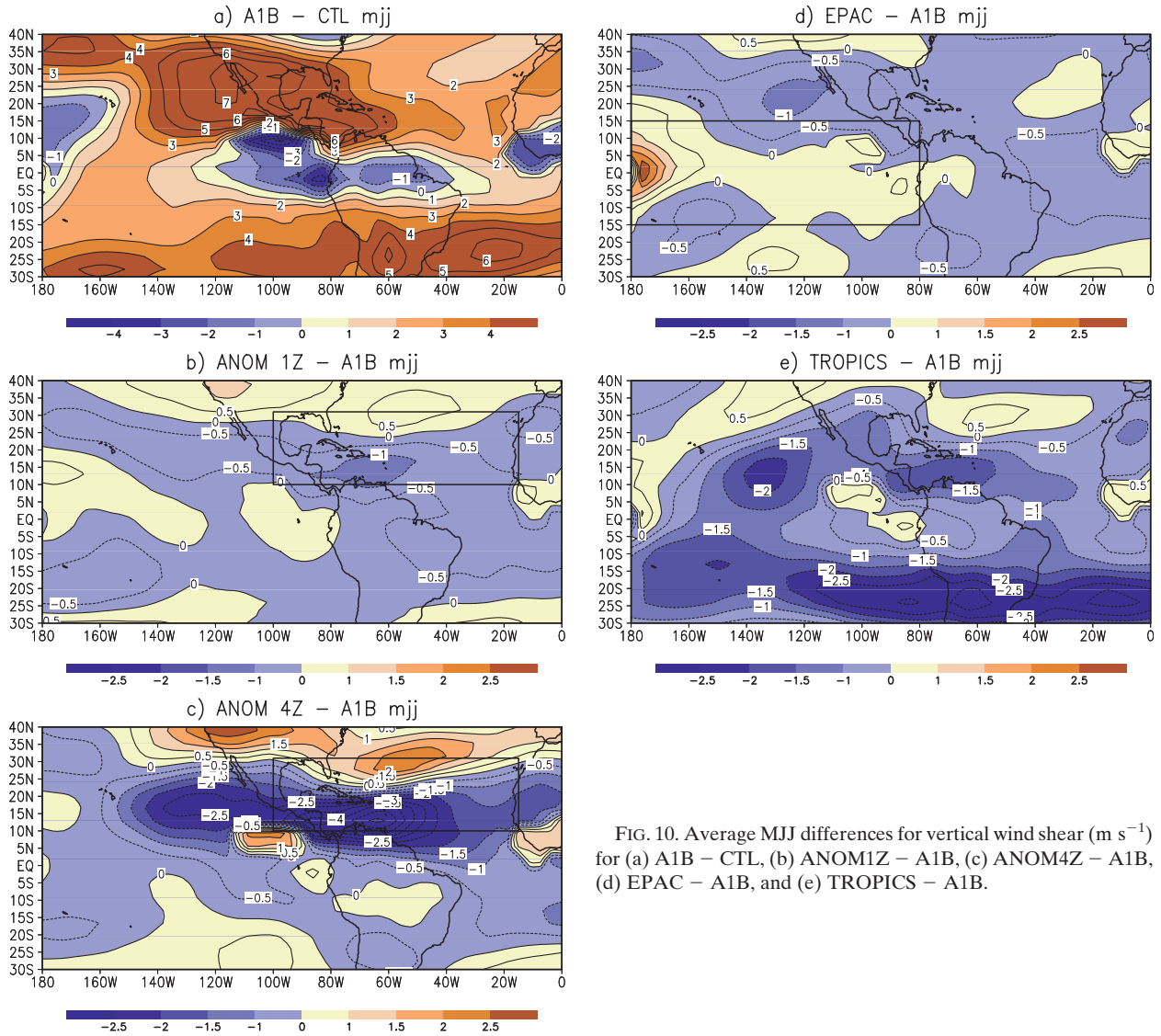


FIG. 10. Average MJJ differences for vertical wind shear ( $\text{m s}^{-1}$ ) for (a) A1B - CTL, (b) ANOM1Z - A1B, (c) ANOM4Z - A1B, (d) EPAC - A1B, and (e) TROPICS - A1B.

over the MA region compared to the A1B simulation (Fig. 5e). Nonetheless, there is still drying over MA compared to the CTL experiment (Fig. 5f). The homogeneous warming  $[(\text{TROPICS} - \text{CTL})/(\text{A1B} - \text{CTL})]$  accounts for 57% of the drying in MJJ and 63% in JJA. These results indicate that the overall warming and perhaps the associated upped ante effect are the most important factors in the drying over MA but that the warming pattern contributes to the drying.

As for the circulation anomalies associated with the uniform SST warming, Fig. 7e shows a decrease in SLP over the TNA and a low-level cyclonic circulation, both similar to the results of the ANOM1Z experiment. In addition, the enhanced southwesterly cross-equatorial flow seen in EPAC is also present in TROPICS, and appears to be enhanced slightly in TROPICS compared to EPAC

owing to its interaction with the anomalous circulation over TNA (e.g., near  $10^{\circ}\text{N}$ ,  $80^{\circ}\text{W}$  and across the Central American isthmus near Panama). Similar to EPAC, the velocity potential differences (Fig. 11b) are dominated by the removal of the ENSO-like warm pattern, with an enhancement of the Pacific Walker circulation compared to the A1B experiment. Here the positive  $\chi$  anomalies are shifted west of the tropical Atlantic, perhaps due to the higher SSTs over this region in the TROPICS experiment compared to A1B. In the TROPICS experiment, the lack of differential warming in the Atlantic and Pacific acts to reduce wind shear (Fig. 10e) compared to the A1B experiment, a result that has been found in observations (Latif et al. 2007). Again, our results suggest that the pattern of SST warming may influence dynamical factors that affect future TC development and intensity.

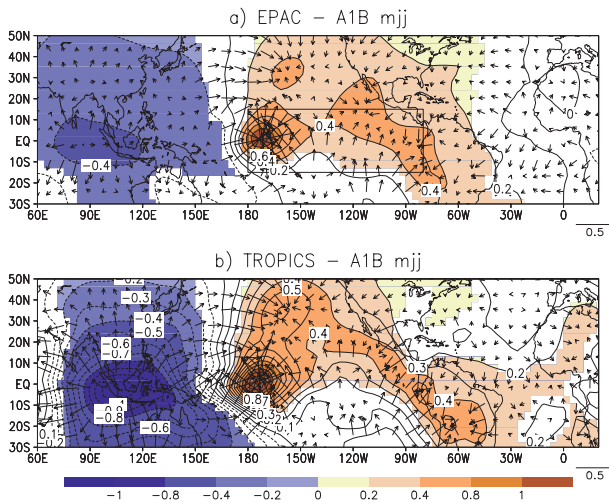


FIG. 11. Average MJJ differences for 200-hPa velocity potential ( $10^6 \text{ m}^2 \text{ s}^{-1}$ ) and divergent winds ( $\text{m s}^{-1}$ ) for (a) EPAC - A1B and (b) TROPICS - A1B. Shaded areas are significant at  $\alpha = 0.1$ .

#### 4. Discussion and conclusions

We find that the ICTP AGCM adequately simulates the spatial pattern of precipitation over the MA region, although precipitation amounts are overestimated. Simulations in which the CMIP3 A1B-20C ensemble-average SSTs are added to the climatological SSTs show drying over the MA region similar to the CMIP3 A1B-20C ensemble-average precipitation response, with precipitation decreases of more than 20% in many areas. Replacing the warming minimum with the zonal-mean SST change (A1B - 20C) in the tropical North Atlantic shows that the reduced warming in the TNA is responsible for 16% and 31% of the overall drying in MA in MJJ and JJA, respectively. A Gill response consistent with an off-equatorial heating anomaly is excited in the region of the applied forcing. When a larger forcing is applied, the drying is ameliorated or reversed. The response is qualitatively similar to the regional response to a large Atlantic warm pool (Enfield et al. 2006; Wang et al. 2007, 2008), but the details differ owing to differences in the shape of the applied SST anomalies. Changing the SST pattern over the eastern Pacific (EPAC) also affects precipitation over the MA region, with changes of 19% and 31% in MMJ and JJA. In that case, there is increased low-level southwesterly cross-equatorial flow that is normally associated with wet conditions over Central America (Hastenrath 1967; Waylen et al. 1996; Peña and Douglas 2002). The TROPICS experiment shows the overall warming of SSTs in the tropics and subtropics is the main contributor of the MA drying, consistent with the “upped ante” effect. All experiments show that the pattern of SST warming

affects vertical wind shear, which may have implications for future changes in tropical cyclones, a source of uncertainty in future climate projections over the MA region (Christensen et al. 2007).

It is important to note that, even without the differential heating of the TNA and eastern tropical Pacific, the MA region is likely to dry (e.g., Neelin et al. 2003; Chou and Neelin 2004; Held and Soden 2006) due to the dominant upped ante effect. Nonetheless, our results show that regional SST variations appear to amplify this future projected drying over Meso-America. We must therefore ask: how much confidence do we have in these regional variations in SST warming? While Leloup and Clement (2009) relate the reduced warming of the TNA to air-sea interactions and increased wind speeds in the TNA, the reduced warming extends over the entire North Atlantic and coincides with a simulated weakening of the Atlantic meridional overturning circulation (Meehl et al. 2007a). It may be that without the Leloup and Clement (2009) mechanism, the reduced warming would be confined to the extratropical North Atlantic. Moreover, there are many features of the tropical mean climate (and of the climate over the eastern tropical Pacific in particular) that are not well represented by models, including the double-ITCZ problem (Lin 2007) and the ENSO cycle in general (e.g., Jin et al. 2008).

More work is needed to identify other contributing mechanisms and sources of uncertainty, particularly focusing on changes in transient and mesoscale phenomena such as easterly waves, tropical cyclones, and regional circulation features including the Caribbean low-level jet. For example, several recent studies have highlighted potential relationships between the strength of the Caribbean low-level jet and easterly wave activity (Méndez and Magaña 2010; Serra et al. 2010), which could be important in this region since many models show an increase in the strength of the CLLJ in the future (Rauscher et al. 2008). Our results may provide some guidance for such experiments. Regional climate modeling studies utilizing a one-way nesting framework should employ large domains that can include the SST forcing over the TNA and eastern tropical Pacific. In addition, the SST warming pattern of the global model should be considered when selecting a model to dynamically downscale, as some models show this effect more than others (Xie et al. 2010).

*Acknowledgments.* SR gratefully acknowledges the support of the U.S. Department of Energy through the LANL/LDRD Program. FK is supported by the ENSEMBLES project, funded by the European Commission’s Sixth Framework Programme (Contract GOCECT-2003-505539). We acknowledge the modeling groups

for providing their data for analysis: the Program for Climate Model Diagnosis and Intercomparison (PCMDI) for collecting and archiving the model output and the JSC/CLIVAR Working Group on Coupled Modelling (WGCM) for organizing the model data analysis activity. The multimodel data archive is supported by the Office of Science, U.S. Department of Energy. We thank Dr. Xunqiang Bi for downloading and processing some of the data used in this work. We thank three anonymous reviewers, whose comments greatly helped to improve the quality and clarity of this paper.

## REFERENCES

- Amador, J. A., 1998: A climatic feature of the tropical Americas: The trade wind easterly jet. *Top. Meteor. Oceanogr.*, **5**, 1–13.
- Bourke, W., 1974: A multi-level spectral model. I. Formulation and hemispheric integrations. *Mon. Wea. Rev.*, **102**, 687–701.
- Bracco, A., F. Kucharski, R. Kallummal, and F. Molteni, 2004: Internal variability, external forcing and climate trends in multi-decadal AGCM ensembles. *Climate Dyn.*, **23**, 659–678, doi:10.1007/s00382-004-0465-2.
- , —, F. Molteni, W. Hazeleger, and C. Severijns, 2005: Internal and forced modes of variability in the Indian Ocean. *Geophys. Res. Lett.*, **32**, L12707, doi:10.1029/2005GL023154.
- Branstator, G., 2002: Circumglobal teleconnections, the jet stream waveguide, and the North Atlantic Oscillation. *J. Climate*, **15**, 1893–1910.
- Chiang, J. C. H., and A. H. Sobel, 2002: Tropical tropospheric temperature variations caused by ENSO and their influence on the remote tropical climate. *J. Climate*, **15**, 2616–2631.
- Chou, C., and J. D. Neelin, 2004: Mechanisms of global warming impacts on regional tropical precipitation. *J. Climate*, **17**, 2688–2701.
- Christensen, J. H., and Coauthors, 2007: Regional climate projections. *Climate Change 2007: The Physical Science Basis*, S. Solomon et al., Eds., Cambridge University Press.
- Clement, A. C., A. C. Baker, and J. Leloup, 2010: Climate change: Patterns of tropical warming. *Nat. Geosci.*, **3**, 8–9, doi:10.1038/ngeo728.
- Cook, K. H., E. K. Vizy, Z. S. Launer, and C. M. Patricola, 2008: Springtime intensification of the Great Plains low-level jet and Midwest precipitation in GCM simulations of the twenty-first century. *J. Climate*, **21**, 6321–6340.
- Covey, C., K. M. AchutaRao, U. Cubasch, P. Jones, S. J. Lambert, M. E. Mann, T. J. Phillips, and K. E. Taylor, 2003: An overview of results from the coupled model intercomparison project. *Global Planet. Change*, **37**, 103–133, doi:10.1016/S0921-8181(02)00193-5.
- Curtis, S., 2002: Interannual variability of the bimodal distribution of summertime rainfall over Central America and tropical storm activity in the far-eastern Pacific. *Climate Res.*, **22**, 141–146.
- Dai, A., 2006: Precipitation characteristics in eighteen coupled climate models. *J. Climate*, **19**, 4605–4630.
- Enfield, D. B., 1996: Relationships of inter-American rainfall to tropical Atlantic and Pacific SST variability. *Geophys. Res. Lett.*, **23**, 3305–3308, doi:10.1029/96GL03231.
- , and D. A. Mayer, 1997: Tropical Atlantic sea surface temperature variability and its relation to El Niño–Southern Oscillation. *J. Geophys. Res.*, **102**, 929–945, doi:10.1029/96JC03296.
- , and E. J. Alfaro, 1999: The dependence of Caribbean rainfall on the interaction of the tropical Atlantic and Pacific Oceans. *J. Climate*, **12**, 2093–2103.
- , S.-K. Lee, and C. Wang, 2006: How are large Western Hemisphere warm pools formed? *Prog. Oceanogr.*, **70**, 346–365, doi:10.1016/j.pocean.2005.07.006.
- Giannini, A., Y. Kushnir, and M. A. Cane, 2000: Interannual variability of Caribbean rainfall, ENSO, and the Atlantic Ocean. *J. Climate*, **13**, 297–311.
- Gill, A. E., 1980: Some simple solutions for heat-induced tropical circulation. *Quart. J. Roy. Meteor. Soc.*, **106**, 447–462.
- Giorgi, F., 2006: Climate change hot-spots. *Geophys. Res. Lett.*, **33**, L8707, doi:10.1029/2006GL025734.
- , and X. Bi, 2005: Updated regional precipitation and temperature changes for the 21st century from ensembles of recent AOGCM simulations. *Geophys. Res. Lett.*, **32**, L21715, doi:10.1029/2005GL024288.
- Gray, W. M., 1984: Atlantic seasonal hurricane frequency. Part I: El Niño and 30 mb quasi-biennial oscillation influences. *Mon. Wea. Rev.*, **112**, 1649–1668.
- Hastenrath, S., 1967: Rainfall distribution and regime in Central America. *Arch. Meteor. Geophys. Bioklimatol.*, **15B**, 201–241.
- , 1976: Variations in low-latitude circulation and extreme climatic events in the tropical Americas. *J. Atmos. Sci.*, **33**, 202–215.
- , 1978: On modes of tropical circulation and climate anomalies. *J. Atmos. Sci.*, **35**, 2222–2231.
- , 2002: The intertropical convergence zone of the eastern Pacific revisited. *Int. J. Climatol.*, **22**, 347–356.
- Held, I. M., and M. J. Suarez, 1994: A proposal for the intercomparison of the dynamical cores of atmospheric general circulation models. *Bull. Amer. Meteor. Soc.*, **75**, 1825–1830.
- , and B. J. Soden, 2006: Robust responses of the hydrological cycle to global warming. *J. Climate*, **19**, 5686–5699.
- Huffman, G. J., R. F. Adler, D. T. Bolvin, and G. Gu, 2009: Improving the global precipitation record: GPCP Version 2.1. *Geophys. Res. Lett.*, **36**, L17808, doi:10.1029/2009GL040000.
- Jiang, H., and E. J. Zipser, 2010: Contribution of tropical cyclones to the global precipitation from eight seasons of TRMM data: Regional, seasonal, and interannual variations. *J. Climate*, **23**, 1526–1543.
- Jin, E. K., and Coauthors, 2008: Current status of ENSO prediction skill in coupled ocean–atmosphere models. *Climate Dyn.*, **31**, 647–664, doi:10.1007/s00382-008-0397-3.
- Kalnay, E., and Coauthors, 1996: The NCEP/NCAR 40-Year Reanalysis Project. *Bull. Amer. Meteor. Soc.*, **77**, 437–471.
- Knutson, T. R., J. J. Sirutis, S. T. Garner, G. A. Vecchi, and I. M. Held, 2008: Simulated reduction in Atlantic hurricane frequency under twenty-first-century warming conditions. *Nat. Geosci.*, **1**, 359–364, doi:10.1038/ngeo202.
- Kucharski, F., F. Molteni, and A. Bracco, 2006a: Decadal interactions between the western tropical Pacific and the North Atlantic Oscillation. *Climate Dyn.*, **26**, 79–91, doi:10.1007/s00382-005-0085-5.
- , —, and J. H. Yoo, 2006b: SST forcing of decadal Indian monsoon rainfall variability. *Geophys. Res. Lett.*, **33**, L03709, doi:10.1029/2005GL025371.
- , A. Bracco, J. H. Yoo, A. M. Tompkins, L. Feudale, P. Ruti, and A. Dell’Aquila, 2009: A Gill–Matsuno-type mechanism explains the tropical Atlantic influence on African and Indian monsoon rainfall. *Quart. J. Roy. Meteor. Soc.*, **135**, 569–579, doi:10.1002/qj.406.
- Latif, M., N. Keenlyside, and J. Bader, 2007: Tropical sea surface temperature, vertical wind shear, and hurricane development. *Geophys. Res. Lett.*, **34**, L01710, doi:10.1029/2006GL027969.

- Leloup, J., and A. Clement, 2009: Why is there a minimum in projected warming in the tropical North Atlantic Ocean? *Geophys. Res. Lett.*, **36**, L14802, doi:10.1029/2009GL038609.
- Lin, J.-L., 2007: The double-ITCZ problem in IPCC AR4 Coupled GCMs: Ocean-atmosphere feedback analysis. *J. Climate*, **20**, 4497–4525, doi:10.1175/JCLI4272.1.
- Magaña, V., J. A. Amador, and S. Medina, 1999: The midsummer drought over Mexico and Central America. *J. Climate*, **12**, 1577–1588.
- , J. L. P. Jorge, L. Vázquez, and J. B. Pérez, 2003: Impact of El Niño on precipitation in Mexico. *Geofis. Int.*, **42**, 313–330.
- Maurer, E. P., J. C. Adam, and A. W. Wood, 2009: Climate model based consensus on the hydrologic impacts of climate change to the Rio Lempa basin of Central America. *Hydrol. Earth Syst. Sci.*, **13**, 183–194.
- Meehl, G. A., and Coauthors, 2007a: Global climate projections. *Climate Change 2007: The Physical Science Basis*, S. Solomon et al., Eds., Cambridge University Press, 747–846.
- , C. Covey, T. Delworth, M. Latif, B. McAvaney, J. F. B. Mitchell, R. J. Stouffer, and K. E. Taylor, 2007b: The WCRP CMIP3 multimodel dataset: A new era in climate change research. *Bull. Amer. Meteor. Soc.*, **88**, 1383–1394.
- Méndez, M., and V. Magaña, 2010: Regional aspects of prolonged meteorological droughts over Mexico and Central America. *J. Climate*, **23**, 1175–1188.
- Molteni, F., 2003: Atmospheric simulations using a GCM with simplified physical parameterizations. I. Model climatology and variability in multi-decadal experiments. *Climate Dyn.*, **20**, 175–191.
- Nakicenovic, N., and R. Swart, Eds., 2000: *Special Report on Emissions Scenarios*. Cambridge University Press, 599 pp.
- Neelin, J. D., C. Chou, and H. Su, 2003: Tropical drought regions in global warming and El Niño teleconnections. *Geophys. Res. Lett.*, **30**, 2275, doi:10.1029/2003GL018625.
- , M. Münnich, H. Su, J. E. Meyerson, and C. E. Holloway, 2006: Tropical drying trends in global warming models and observations. *Proc. Natl. Acad. Sci. USA*, **103**, 6110–6115, doi:10.1073/pnas.0601798103.
- Peña, M., and M. W. Douglas, 2002: Characteristics of wet and dry spells over the Pacific side of Central America during the rainy season. *Mon. Wea. Rev.*, **130**, 3054–3073.
- Rauscher, S. A., A. Seth, B. Liebmann, J.-H. Qian, and S. J. Camargo, 2007: Regional climate model-simulated timing and character of seasonal rains in South America. *Mon. Wea. Rev.*, **135**, 2642–2657.
- , F. Giorgi, N. S. Diffenbaugh, and A. Seth, 2008: Extension and intensification of the Meso-American mid-summer drought in the twenty-first century. *Climate Dyn.*, **31**, 551–571, doi:10.1007/s00382-007-0359-1.
- Rodgers, E. B., R. F. Adler, and H. F. Pierce, 2001: Contribution of tropical cyclones to the North Atlantic climatological rainfall as observed from satellites. *J. Appl. Meteor.*, **40**, 1785–1800.
- Ropelewski, C. F., and M. S. Halpert, 1987: Global and regional scale precipitation patterns associated with the El Niño/Southern Oscillation. *Mon. Wea. Rev.*, **115**, 1606–1626.
- Serra, Y. L., G. N. Kiladis, and K. I. Hodges, 2010: Tracking and mean structure of easterly waves over the Intra-Americas Sea. *J. Climate*, **23**, 4823–4840.
- Sobel, A. H., I. M. Held, and C. S. Bretherton, 2002: The ENSO signal in tropical tropospheric temperature. *J. Climate*, **15**, 2702–2706.
- Stephenson, D. B., and I. M. Held, 1993: GCM response of northern winter stationary waves and storm tracks to increasing amounts of carbon dioxide. *J. Climate*, **6**, 1859–1870.
- Vecchi, G. A., and B. J. Soden, 2007: Increased tropical Atlantic wind shear in model projections of global warming. *Geophys. Res. Lett.*, **34**, L08702, doi:10.1029/2006GL028905.
- Wang, C., 2007: Variability of the Caribbean low-level jet and its relations to climate. *Climate Dyn.*, **29**, 411–422, doi:10.1007/s00382-007-0243-z.
- , and S.-K. Lee, 2007: Atlantic warm pool, Caribbean low-level jet, and their potential impact on Atlantic hurricanes. *Geophys. Res. Lett.*, **34**, L02703, doi:10.1029/2006GL028579.
- , —, and D. B. Enfield, 2007: Impact of the Atlantic warm pool on the summer climate of the Western Hemisphere. *J. Climate*, **20**, 5021–5040.
- , —, and —, 2008: Climate response to anomalously large and small Atlantic warm pools during the summer. *J. Climate*, **21**, 2437–2450.
- Waylen, P. R., C. N. Caviedes, and M. E. Quesada, 1996: Interannual variability of monthly precipitation in Costa Rica. *J. Climate*, **9**, 2606–2613.
- Xie, P., and P. A. Arkin, 1996: Analysis of global monthly precipitation using gauge observation, satellite estimates, and numerical model predictions. *J. Climate*, **9**, 840–858.
- Xie, S.-P., C. Deser, G. A. Vecchi, J. Ma, H. Teng, and A. T. Wittenberg, 2010: Global warming pattern formation: Sea surface temperature and rainfall. *J. Climate*, **23**, 966–986.